Applied Surface Science 478 (2019) 1081–1089

Contents lists available at ScienceDirect

Applied Surface Science

journal homepage: www.elsevier.com/locate/apsusc

Full length article

ZnO/GaN heterojunction based self-powered photodetectors: Influence of interfacial states on UV sensing

Monu Mishra[a,b], Abhiram Gundimeda[b,c], Tushar Garg[d], Ajit Dash[e], Susanta Das[f], Vandana[b], Govind Gupta[a,b,*]

[a] Academy of Scientific and Innovative Research, CSIR-NPL Campus, Dr. K.S. Krishnan Marg, New Delhi 110012, India
[b] Advanced Materials and Devices Division, CSIR-National Physical Laboratory, Dr. K.S. Krishnan Marg, New Delhi 110012, India
[c] Cambridge Centre for Gallium Nitride, Department of Materials Sciences and Metallurgy, University of Cambridge, Cambridge CB3 0FS, United Kingdom
[d] Department of Physics, Institute of Chemical Technology, Matunga, Mumbai 400019, India
[e] Department of Electronics and Communication, National Institute of Science and Technology, Berhampur, Odisha 761008, India
[f] Department of Physics & Mathematics, Faculty of Science, Sri Sri University, Cuttack 754006, Odisha, India

ARTICLE INFO

Keywords:
GaN
ZnO
Heterostructure
Interface
Valence band offset etc.

ABSTRACT

Gallium Nitride (GaN) and Zinc Oxide (ZnO) are well established semiconductors with their heterostructures opening avenues for the future of next generation sensing and opto-electronics technologies due to their low lattice mismatch and high exciton energy. ZnO/GaN heterostructure based ultraviolet photodetectors with complimentary material properties are expected to yield optimum efficiency, though their performance has remained low due to challenges related to interfacial properties. Inadequate analysis of ZnO/GaN interfacial properties/states viz. electronic structure, band offsets, localized charge density and defect states associated with overlayer (i.e. ZnO) thickness, and their influence on device performance has remained as an underestimated issue. Interestingly, literature reports a huge anomaly in the valence band offset (VBO) at ZnO/GaN interfaces, which being an effective measure of charge transport assist in the optimization of photodetector efficiency. Therefore, in the present report, we have fabricated ZnO/GaN heterostructure (with variable ZnO thickness) based Schottky barrier photodectors and investigated the dependence of photosensitivity & other device parameters on interfacial states/properties. We have witnessed a peak responsivity & detectivity of 225 mA/W^{-1} & 4.83 ($\times 10^{13}$) Jones and a high speed photoswitching associated with the band offset, barrier height & defect states at the ZnO/GaN heterojunction. The underlying scientific phenomenon (e.g. interfacial dipole strength, charge accumulation etc.) leading to perturbations & discontinuities in interfacial/electronic states were also correlated and discussed in detail.

1. Introduction

Zinc Oxide (ZnO) and Gallium Nitride (GaN) are well established wide bandgap semiconducting materials (ultraviolet regime) belonging to wurtzite crystal structure (4 atoms per unit cell, 9 optical & 3 acoustic phonon modes) with potential future in next generation micro/opto-electronics, sensing and photo-voltaic/catalytic devices [1,2]. ZnO and GaN exhibit similar properties like direct band gap (~3.37 & 3.41 eV), low lattice mismatch (1.9%), strong cohesive energy (1.89 & 9.16 eV^2), large exciton binding energy (60 & 24 meV) and strong inherent spontaneous polarization (0.047 & 0.029C/m^2), respectively [3–5]. Thus, combining the merits of these materials, ZnO/GaN heterostructures offering enhanced light absorption [6] are employed for the fabrication of efficient light emitting diodes (LEDs) [7], laser diodes [8], standing acoustic wave devices [9], toxic gas sensors [10] etc. Also, the quest of a robust, ultrasensitive and highly responsive ultraviolet (UV) photodetector (PD) can be fulfilled using the heterostructure of ZnO and GaN, where the large and stable exciton energy of ZnO coupled with unique properties of GaN can open avenues for the fabrication of efficient devices [11–13]. Essentially, the performance of a heterostructure based device is governed via interfacial properties (e.g. band offset, bending, barrier height etc.) facilitating effective carrier transport across the junction. The importance of interfacial properties can be visualized via previous (and recent) reports where the responsivity of the photodetectors fabricated using ZnO/GaN heterostructure was quiet low compared to the expectations [12–14]. The inadequate and anomalous studies of electronic properties at the ZnO/GaN interfaces, which governs the effective charge transport across the

* Corresponding author at: Academy of Scientific and Innovative Research, CSIR-NPL Campus, Dr. K.S. Krishnan Marg, New Delhi 110012, India.
E-mail address: govind@nplindia.org (G. Gupta).

https://doi.org/10.1016/j.apsusc.2019.01.192
Received 3 December 2018; Received in revised form 2 January 2019; Accepted 22 January 2019
Available online 10 February 2019
0169-4332/ © 2019 Elsevier B.V. All rights reserved.

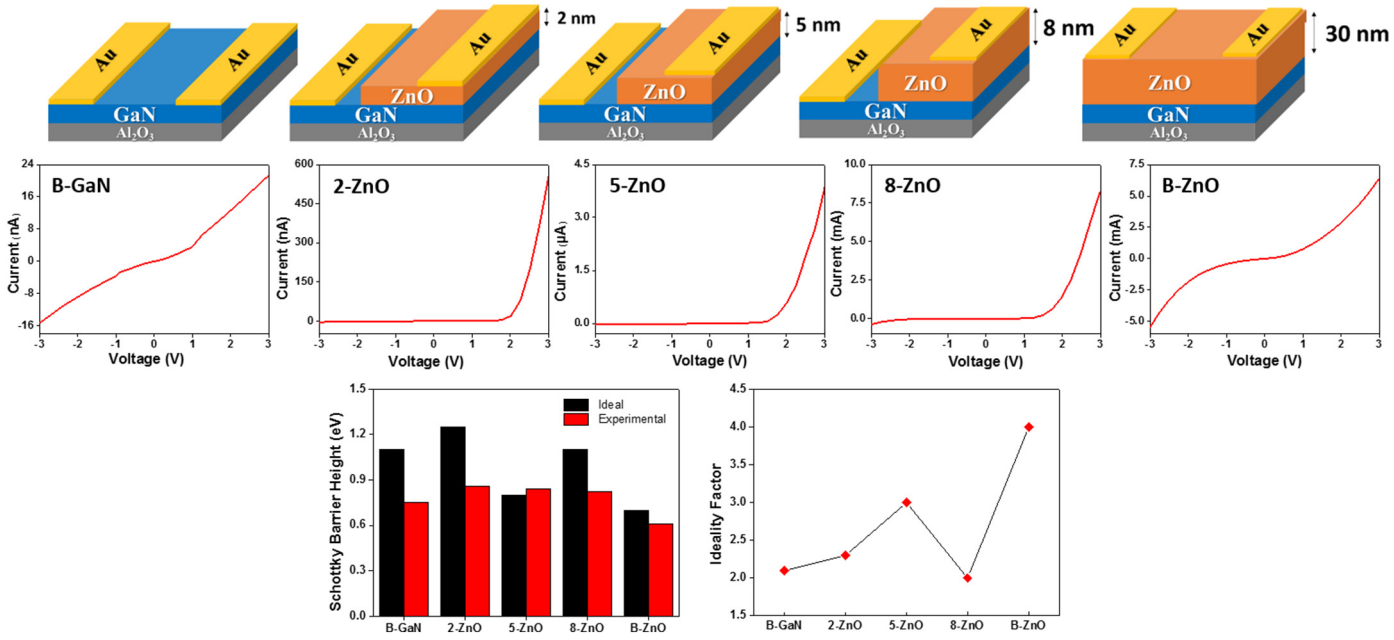

Fig. 1. Schematic representation, I-V curves and calculated values of Schottky barrier height ad ideality factors of the fabricated devices.

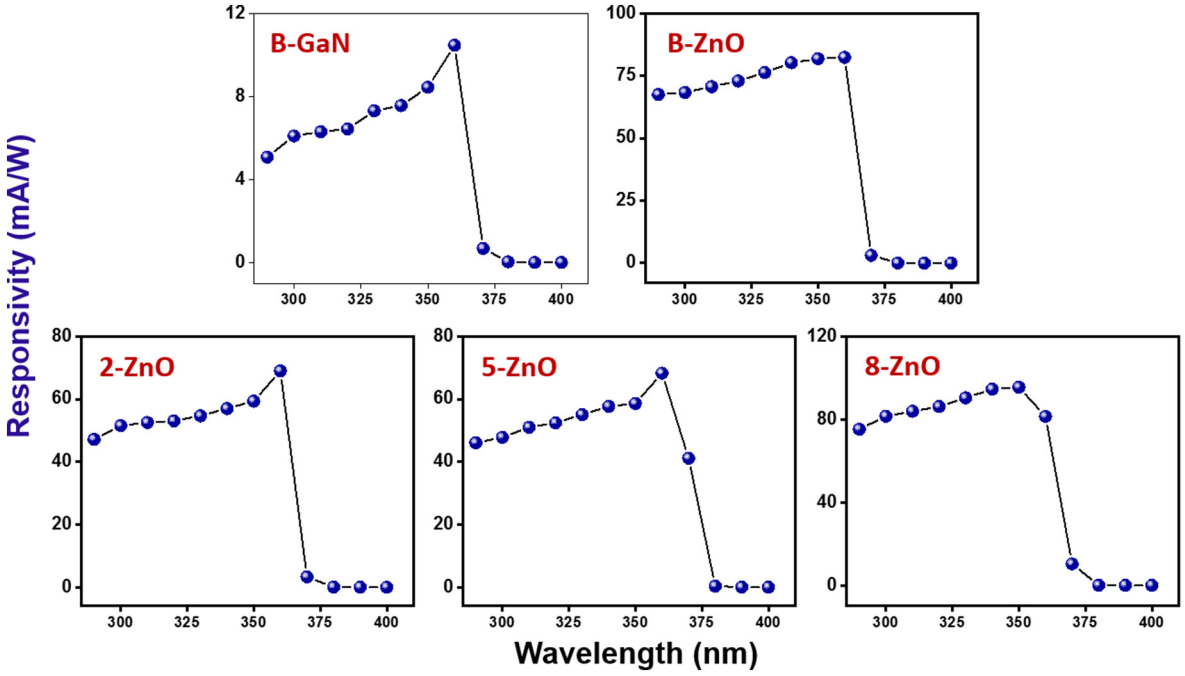

Fig. 2. Responsivity of the fabricated devices under different incident radiations at self-powered operation condition.

junction, was the major cause behind the poor performance/efficiency of ZnO/GaN heterostructure based devices.

ZnO/GaN heterojunction exhibits a Type II (staggered) band alignment which is extremely beneficial for energy harvesting and photon detection in optoelectronic/photonic devices [15–19]. In Type II heterojunctions, electron and hole wave functions peak in different layers, leading to enhanced device performance operating at wavelengths beyond their conventional band gap limits [17–21]. Despite of its critical importance and extensive research of over 2 decades, literature report a huge anomaly (0.8–2.2 eV) [8,15,22–24] in the valence band offset (VBO) value at the ZnO/GaN interface. The VBO at material interface depends on various aspects viz. surface states (defects, chemical species, electron/hole accumulation etc.), polarization, interface dipole/energy, charge screening and thickness of the overlayer. Therefore, the aforementioned factors should be taken under consideration to develop a deeper insight of phenomenon occurring that lead to discontinuities/perturbations in measured VBOs, Schottky barrier height (SBH) and ultimately the device performance. It illustrates that an in-depth analysis of interfacial defect states will help to understand underlying science and contribute in enhancing the reliability and concreteness of the obtained results. Here, in the present article, to investigate the influence of electronic/chemical/defect & interfacial states on the performance of ZnO/GaN heterostructure based Schottky barrier photodetectors, we have performed a detailed analysis of the performance of ZnO/GaN based photodetectors. The analysis was followed by correlation with material properties, carrier dynamics, defect

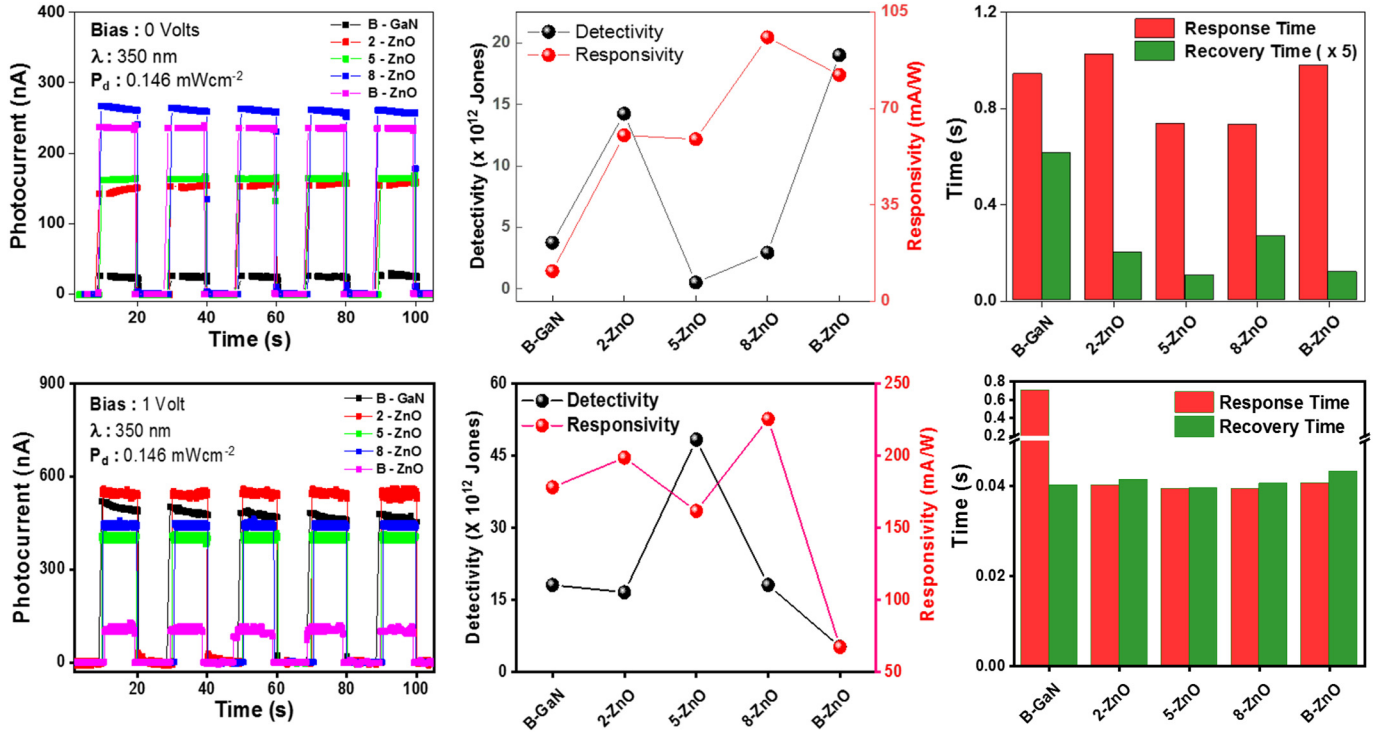

Fig. 3. Photoresponse, responsivity, detectivity, response and recovery time of the devices under different at 0 V and 1 V applied bias.

Table 1
Figure of merit parameters of the fabricated Schottky barrier diodes under different external bias conditions.

	B-GaN	2-ZnO	5-ZnO	8-ZnO	B-ZnO	Bias (V)
Responsivity (mAW^{-1})	10.9	60.2	58.8	95.8	82.2	0
	178.0	198.6	161.6	225.4	67.3	1
Detectivity ($x10^{12}$ Jones)	3.7	14.2	0.5	2.9	19.0	0
	18.1	16.6	48.3	18.1	5.2	1
Response time (ms)	942.4	1023.5	735.7	731.6	976.3	0
	704.3	40.1	39.3	39.3	40.6	1
Recovery time (ms)	122.8	40.1	40.5	53.1	42.6	0
	43.6	41.4	39.5	40.7	43.2	1

Table 2
Comparison of obtained responsivity with previously reported values.

	Responsivity (mAW^{-1})	Reference
ZnO (varied thickness)/GaN	225	This work
n-ZnO nanorods/*i*-ZnO/p-GaN	139	[11]
n-ZnO nanorods/i-MgO/p-GaN	160	[25]
ZnO nanoarray/CdS/GaN	176	[26]
n-ZnO nanoarray/n-GaN	34	[27]
Al-ZnO/GaN	120	[28]
Multiwalled carbon nanotubes/ZnO nanowires/p-GaN	6	[29]

states and current conduction is derived to realize the underlying science determining the surface & interfacial properties and ultimately the device efficiency.

2. Material and characterization

A 3.5 μm thick highly crystalline GaN epilayer (2theta-omega FWHM = 226 arcsec) grown on sapphire along polar (0001) direction was employed as substrate for the experiment. GaN epilayer were degreased in isopropyl alcohol and ultra-sonicated in acetone for 10 min each to remove the surface contaminants prior to the overlayer growth. ZnO/GaN sharp interfaces were fabricated via growth of ZnO films with varied thickness (2, 5, 8 & 30 nm) on cleaned GaN substrates by atomic layer deposition (ALD) reactor (M/s Picosun, Model R200) at a substrate temperature of 300 °C under identical conditions using pre-optimized parameters. The samples are abbreviated as B-GaN, 2-ZnO, 5-ZnO, 8-ZnO and B-ZnO for bulk GaN, 2 nm ZnO/GaN, 5 nm ZnO/GaN, 8 nm ZnO/GaN and bulk ZnO structures respectively. Metallic gold contacts (~80 nm) were deposited on the heterostructures using physical vapor deposition technique to fabricate Schottky barrier diodes and investigate the current conduction mechanism across the junction. Photodetection measurements were carried out in DC mode under continuous illumination of monochromatic light (with Xenon/Quartz-Halogen lamps) at different wavelengths using a TMc 300 monochromator having a resolution of 0.1 nm. To correlate the performance of the UV PDs with electronic properties, high resolution X-Ray photoemission spectroscopic (XPS) measurements were performed in a multiprobe surface analysis system (Scienta Omicron, Germany) using monochromatic AlKα (1486.7 eV) radiation source [25]. Optical response and defect state analysis of the devices were investigated via a Photoluminescence (PL) Fluorescence spectrometer FLS980-d2d2 (Edinburgh Instruments, United Kingdom) equipped with a He–Cd continuous wave laser operating at an excitation wavelength of 325 nm and emission arm equipped with a standard Visible PMT.

3. Results and discussion

The approach for the experiment was to fabricate ZnO/GaN heterostructure (with varied ZnO thickness) based Schottky barrier PDs, investigate their performance/efficiency followed by an in-depth analysis of interfacial properties/states & underlying science/phenomenon using state of the art characterization tools. The overlayer thickness in the ZnO/GaN heterostructure was restricted to 8 nm, as the probing depth of XPS (employed for electronic structure analysis) is ~8–10 nm only. The schematic representation of the fabricated devices along with their RT current-voltage (I-V) curves is shown in Fig. 1. It was witnessed

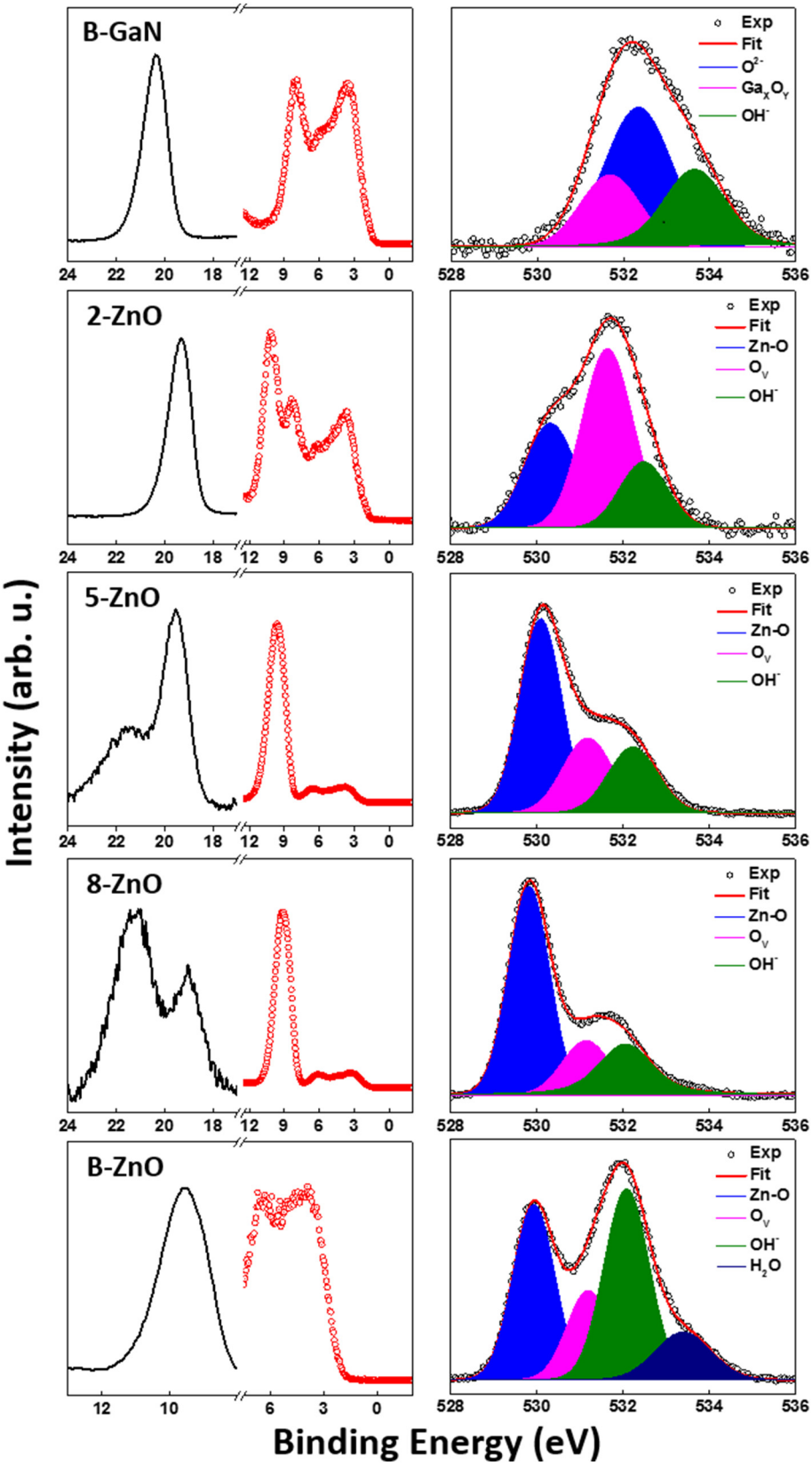

Fig. 4. Ga (3d), Zn (3d), Valence band and deconvoluted O (1s) spectra of the heterostructures.

that B-GaN film display a Schottky (rectifying) behaviour with 21 nA of current in forward bias condition (at 3 V). However, the rectifying behaviour was transformed into Schottky barrier diode (SBD) characteristics for 2, 5 and 8-ZnO followed by a drastic improvement in current conduction. Interestingly, the threshold voltage of the devices were also decreased from 2.1 V to 1.5 V from 2-ZnO to 8-ZnO revealing easier extraction of charge carriers. The forward current was obtained to be 0.6, 4.0 and 8200 μA for 2, 5 and 8-ZnO displaying an increment of 10^5

Table 3
Core level, VB positions and quantified contribution of the deconvoluted O (1s) components.

		B-GaN	2-ZnO	5-ZnO	8-ZnO	B-ZnO
O (1s)	Ga (3d) (eV)	20.2	19.4	19.5	19.1	–
	Zn (3d) (eV)	–	10.1	9.6	9.1	9.6
	VBM (eV)	1.8	2.0	2.3	1.8	2.1
	Zn-O (%)	–	30	54	60	33
	O^{2-}/O_V (%)	23	52	25	18	17
	OH^- (%)	49	18	21	22	38
	H_2O (%)	28	–	–	–	12

times in comparison to B-GaN. Further, the I-V curves divulged Schottky behaviour for B-ZnO pursuing a forward current of 6400 μA which is slightly lower then 8-ZnO (8200 μA). The increment in forward current signifies higher number of charge carriers generated in the device with increment in ZnO thickness. To further explore the properties of the fabricated devices, a deeper insight into the current conduction mechanism is required. According to the thermionic theory, the current conduction across a SBD is expressed as [26]:

$$I = I_S[exp(qV/nkT) - 1] \quad (1)$$

where,

$$I_S = AA^*T^2 exp(-q\varphi_{B0}/kT) \quad (2)$$

here, I is the diode current, I_S is the saturation current, q is the electronic charge, V is the applied bias, T is the absolute temperature, n is the ideality factor, k is the Boltzmann constant, A is the effective Schottky area, A* is the effective Richardson coefficient of 26.2 $Acm^{-2}K^{-2}$ and φ_{B0} is the apparent zero bias Schottky barrier height. Further the value of ideality factor was calculated via the slope of log(I-V) graph (in thermionic emission) using the following relation [26]:

$$n = \frac{q}{2.303kT}\left(\frac{dv}{d(\log I)}\right) \quad (3)$$

The value of saturation current (I_S) was obtained from the y-intercept in the log I-V graph, and the Schottky barrier height (φ_{B0}) was calculated as:

$$\varphi_{B0} = \frac{kT}{q}\ln\left(\frac{AA^*T^2}{I_s}\right) \quad (4)$$

The procedure for the calculation of barrier height and ideality factor is well demonstrated in Fig. S1 of supplementary material. We calculated the φ_{B0} values via two different approaches and labelled as: Ideal and Experimental. Since φ_{B0} is the difference between metal work-function and the electron affinity (EA) of semiconductor. The Ideal value of φ_{B0} (black histograms in Fig. 1) was calculated using the difference between work-function of gold (5.1 eV) and the EA of GaN. The EA of the heterostructures were calculated via UPS measurements and shown in Fig. S2 of supplementary material. However, the experimental value was calculated using the slope (and Eq. (4)) derived from the I-V curves in the thermionic emission range (0.0–0.5 V) and represented as red histograms in Fig. 1. It was evident that the ideal value of φ_{B0} is higher than its experimental value in all devices except 5-ZnO. The ideal value for φ_{B0} varied between 0.7 and 1.3 eV, while the experimental value were more reliable and remained within 0.6–0.9 eV. The perturbations obtained in the φ_{B0} of GaN were attributed due to the presence of surface/interface states, contacts inhomogeneity, defect states and most importantly FL pinning [26]. Besides, the presence of surface/interface dipole generates an interface potential which hinders the performance of SBD and thereby alter the barrier height. The ideality factor of the fabricated SBD varied between 2 and 4, although, the value of n for B-GaN and B-ZnO has no physical significance (due to the absence of diode characteristics). In SBD, the value of n for 2, 5 and 8-ZnO was obtained to be 2.1, 3.0 and 2.0. Interestingly, the ideality factor for 5-ZnO reflected an adverse behaviour. Therefore, we analysed the electronic structure of the SBDs in detail to explore the reason behind such odd value of ideality factor (as explained in next sections).

In order to realize the performance of fabricated Schottky barrier diodes for photo-sensing applications, the devices were subjected to UV detection measurements. All the important figure of merit device parameters (e.g. responsivity, detectivity, switching time etc.) which governs the efficiency/reliability of a UV detector, were calculated using standard procedure [27,28]. It was observed that the spectral response curves of the fabricated Schottky barrier UV PDs (as shown in Fig. 2) revealed a good photodetection in the UV regime (upto 380 nm) with a visible-blind photosensitivity under self-powered operation mode [1]. The peak responsivity of the UV PDs obtained in the wavelength range of 360–380 nm (at 0 V bias), was attributed to the bandgap of GaN and ZnO (corresponding to 3.37–3.41 eV). However, the photoresponse below the bandgap (i.e. 280–360 nm) of material could be attributed to two-photon absorption (TPA) leading to photon absorption in forbidden gap. The TPA phenomenon in predominant in III-V materials (and other wideband gap materials) and Schottky barrier heterostructures where the dimension of device is narrowed [1,29–34] (associated with the nano-regime thickness of the overlayer in present scenario).

Further, the performance of the UV PDs was compared at two different external bias conditions (0 V and 1 V). Interestingly, all the devices divulged self-powered operation (i.e. 0 V external bias) along with an increment in responsivity & detectivity at applied bias (i.e. 1 V) as shown in Fig. 3. The figure of merit parameters of the UV PDs at 0 V and 1 V applied bias is tabulated in Table 1 for better comparison. The analysis revealed that the responsivity as well as detectivity of the PDs increased significantly with applied bias (i.e. 1 V). The responsivity of 8-ZnO based UV PDs was highest at both self-powered (95.8 mAW^{-1}) as well applied bias (225.4 mAW^{-1}) condition with respect to other devices. On the other hand B-ZnO (at 0 V) and 5-ZnO (at 1 V) disclosed highest detectivity, while least responsivity was obtained for 5-ZnO (at

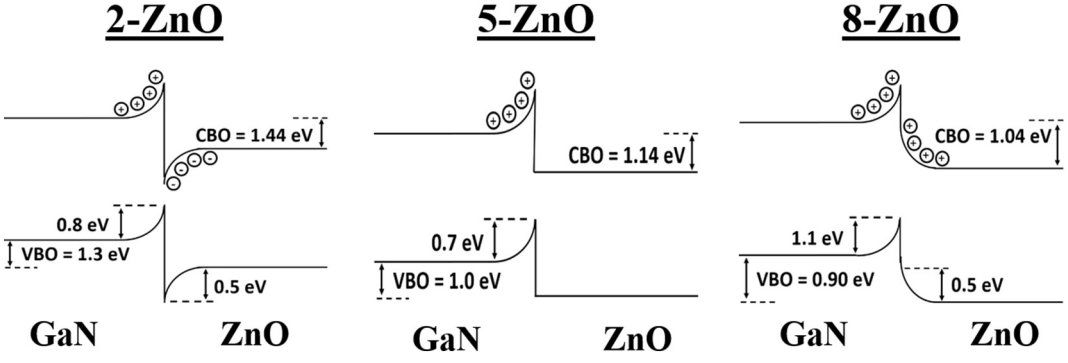

Fig. 5. Band bending and measured valence band offset at the ZnO/GaN interfaces.

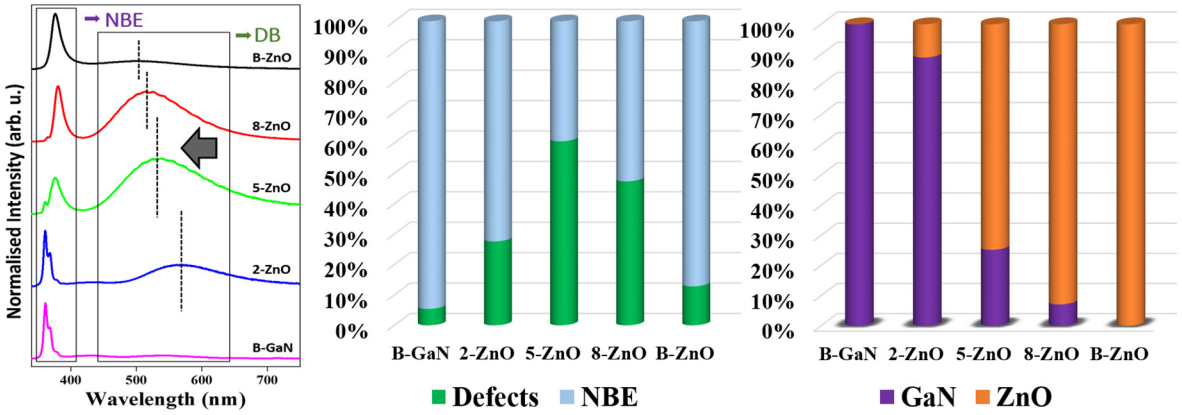

Fig. 6. Room temperature PL spectra and intensity ratio of NBE to Defect states and GaN & ZnO (NBE) in the grown heterostructures.

0 V) and B-ZnO (at 1 V), respectively. The obtained values of responsivity were much higher than previously reported values on ZnO/GaN heterostructures (including hybrid structures) based UV PDs (see Table 2). Also, the fabricated UV PDs divulged faster photoswitching rate with a response & recovery time ranging from of milliseconds to few hundred microseconds (Table 1). Though, the response time of the devices was higher under self-powered operation, it was reduced drastically at applied bias (i.e. 1 V). The higher response time of the UV PDs under self-powered operation mode was ascribed to absence of a driving force (or potential) associated with external bias which is present at 1 V.

In order to develop a deeper insight of underlying science to understand the reason behind increment in responsivity/detectivity with ZnO thickness, we correlated it with the surface/interfacial properties (band offset, bending, defects etc.). The XPS spectrum of Ga (3d) & Zn (3d) core level (CL) along with valence band (VB) spectra with respect to binding energy (BE) is represented in Fig. 4 (position/contribution tabulated in Table 3). The spectra shows peak at ~9.6 eV & ~20.0 eV corresponding to Zn (3d) & Ga (3d) CLs while the additional peak located at ~22.0 eV observed in 5-ZnO and 8-ZnO was assigned to O (2s) CL. To identify the nature of oxidation states and the expanse of oxygen vacancies, O (1s) CL spectra (located at ~531 eV) of the grown heterostructures was deconvoluted into 5 components viz. Zn-O, Ga_XO_Y, Ga_2O_3 (O^{2-}), Oxygen vacancies (Ov), Hydroxyl species (OH^-) and adsorbed water molecules (H_2O) at their respective BE positions [35–37]. The most interesting observation witnessed was the suppression of oxygen vacancies (O_V) associated defect states with ZnO thickness. The results divulged that the increment in ZnO thickness (from 2 nm to 8 nm) lead to reduction in O_V (52% to 18%) and increment in Zn-O associated peaks (30% to 60%) in the deconvoluted O (1s) CL. Though, the contribution of hydroxyl species (OH^-) remained in the close vicinity of each other (from 18% to 22%).

To securitize the degree of near surface localized band bending (BB), the BE position of Ga (3d) and Zn (3d) CLs were employed to calculate the BB on either side of the interface [38]. Though, for developing a better insight of BB at the interface, it is essential to explain about electronic states at the interface developed form surface states (and induced FL pinning) of GaN and the charge transfer from ZnO. Surface states originate from the interaction of unpaired electrons in dangling bonds of surface atoms due to termination of lattice periodicity which possess different and independent energetics/electronic structure from the bulk semiconductor (as the density of surface states is very large i.e. $\sim 10^{15}\,cm^{-2}$). An upwards BB indicates accumulation of holes (i.e. acceptor states) while downwards BB is a signature of accumulation of electrons (i.e. donor states). Though, a flat band condition signifies absence of charge transfer from bulk to surface. Such phenomenon occurs most specifically in materials with inherent polarization effect (quantum confined stark effect) where the seeding polarity (and surface termination) decides the direction/nature of polarization induced charge accumulation (i.e. electrons or holes) on the surface/interface [38]. In GaN, the direction of spontaneous polarization (dominating total polarization) is directed from bulk to surface in Ga-polar and surface to bulk in N-polar GaN film. It yields negatively bound charges on the surface of Ga-polar and positive bound charges on the surface of N-polar GaN film [39] which can be observed via shift in CLs. The obtained results demonstrated an upwards BB in GaN interfacial region, while the BB along ZnO region varied indifferently. Initially at 2 nm ZnO thickness, a downwards BB was perceived, which was transformed to a flat band (FB) and an upwards BB state with increase of overlayer thickness to 5 nm and 8 nm, respectively. The schematic representation of BB (and band offsets) at the interfaces is shown in Fig. 5. The perturbation in the nature of BB is relative to the pinning of FL in GaN and the contribution of O_V in ZnO. The FL was pinned at 1.8 eV above the VB in GaN (bulk) which reveal N-rich [40] (i.e. accumulation of acceptor states) surface while the concentration of O_V in ZnO varied differently. GaN displayed formation of depletion layer on the surface persistently while BB of ZnO showcased formation of accumulation, flat band as well as depletion region depending on overlayer thickness. The mechanism of BB along ZnO interface can be explained on the basis of its atomic structure and bonding states. First, the wurtzite ZnO crystal structure has a four-fold coordination, the higher concentration of O_V would lead to enhanced donor states at the interface originating from excess zinc (which reduced with reduction in the concentration of O_V) and vice versa. The excess zinc in the ZnO may act as interstitial centres (Zn_i) and assist in the development of donor like states. Second, since metal pursue small screening length (of atomic sizes) in comparison to semiconductors [41], the conversion of accumulation layer to flat band and depletion layer with reduction in the concentration of O_V and increment in ZnO thickness is acceptable. Since the accumulation of excess or deficit charges (i.e. donor or acceptor states) at the interface would lead to interface instability, charge compensation via reconstruction at the interface to neutralise charge effects (minimum interface energy) takes place. The interfacial reconstruction generates interface dipoles with perturbed energetics could alter the interfacial band alignment (and band offsets) which is reflected in the obtained results.

The Surface barrier height ($e\phi_B$), which is the difference between conduction band minimum and FL was calculated to be 1.4, 1.1 & 1.6 (± 0.1) eV for 2-ZnO, 5-ZnO & 8-ZnO, respectively. The variation in surface barrier height could be attributed to the presence of donor/acceptor states or charges neutrality conditions at the interface of heterostructure [42]. It is evident that 5-ZnO pursue minimum surface barrier height (i.e. 1.1 eV) while it was highest (i.e. 1.6 eV) for 8-ZnO which could be attributed to the flat-band structure at 5-ZnO and acceptor states at 8-ZnO interfacial region. The valence band offset (VBO) in the interfacial region was calculated by using following equation

[43]:

$$\Delta E_V = \Delta E_{CL} - (E_{3d} - E_{VBM})^{ZnO} + (E_{3d} - E_{VBM})^{GaN} \quad (5)$$

where,

$$\Delta E_{CL} = ((E_{3d})^{ZnO} - (E_{Ga3d})^{GaN})^{ZnO/GaN} \quad (6)$$

The ΔE_{CL} is the CL energy separation between Zn (3d) and Ga (3d) spectra of the grown ZnO/GaN heterostructures while $(E_{CL} - E_{VBM})^{Material}$ is separation between CL and VBM of the bulk ZnO and GaN samples. The VBO values calculated for 2-ZnO, 5-ZnO and 8-ZnO was observed to be 1.3, 1.0 and 0.9 (± 0.1) eV corresponding to CBO of 1.4, 1.1 and 1.0 (± 0.1) eV, respectively. The results decipher the disparity of calculated VBO at ZnO/GaN interface in the reported literature and support the argument of perturbation in VBO due to overlayer thickness and interface dipole. Besides, it can also be validated that the ZnO/GaN interface has a Type-II band alignment along with VBO nearly equal to 1.0 eV. It is noteworthy to mention that the band offset doesn't depend on crystal structure but on atomic density which governs the interface dipole and hence lead in discontinuities in measured VBO.

For the investigation of defect states at the interface, room temperature PL measurements of the heterostructures were performed (as shown in Fig. 6). The peaks located at 361 and 377 nm were attributed to the characteristic near band edge (NBE) emission from GaN and ZnO film, respectively. A broad defect band (DB) ranging from 400 to 700 nm, associated with the inherent defect states and corresponding to the dominating blue, green and yellow luminescence (BL, GL & YL) was also observed [2,44]. The intensity of peak located at 361 nm (corresponding to GaN) was decreased with increment in overlayer thickness displaying strong emission from ZnO. It is evident that B-GaN pursue traces of BL (432 nm) & YL (548) along with donor-acceptor pair (368 nm), though GL (504 nm) was predominant in B-ZnO. The origin of DB in GaN and ZnO was attributed to the presence of inherent defect states associated with point defects, dislocations, vacancies, interstitials, dangling bonds etc. [44–46]. Since identical GaN epilayer used for all growth, perturbation in DB was assumed to be originated from the ZnO/GaN interface (including GaN surface reactions) or ZnO itself. The DB analysis demonstrates that B-GaN pursue BL and YL at 432 and 548 nm respectively while it display a red shift of 12 nm for 2-ZnO. DB at 560 nm for 2-ZnO is a superposition of luminescence from defects of GaN and ZnO, leading to a yellowish-green emission at 560 nm [47,48]. Further, a blue of shift of 28, 44 and 56 nm was observed for 5-ZnO, 8-ZnO and B-ZnO revealing strong GL with increment in ZnO thickness [48]. Though the intensity ratio of NBE and GL (I_{NBE}/I_{GL}) varied indifferently and showed maximum value for 5-ZnO sample. Since the origin of the dominating defect states of ZnO (i.e. GL) remained in debate, it was ascribed to various factors such as oxygen & zinc vacancies (V_O & V_{Zn}), interstitials (O_i & Zn_i), antisites (Zn_O) and transitions (Zn_i to V_{Zn}) though many factors may be involved simultaneously [44]. The XPS analysis revealed that the concentration of O_V decreases from 2-ZnO to B-ZnO along with reduction in donor states (i.e. excess zinc). The excess zinc (originating due to O_V) leads to the development of interstitial centres (Zn_i) forming shallow levels (concentration decreasing 5, 8 and B-ZnO) are highly responsible for GL in ZnO [49].

The PL data revealed two major questions as: 1) why there is a shift in DB and 2) the reason behind the fluctuation in the intensity of DB. Since the origin of DB in ZnO is mostly associated with vacancies and interstitials, the variation in the concentration of these defect states led to observed shifts in the DB. Initially at lower ZnO thickness, the concentration of O_V is very high which indicates that Oxygen leaves the intrinsic site and occupies the interstitial site (O_i) along with the formation of Zn_i due to limited surface reaction and unsaturated coordination. These shallow level and deep acceptor defector type of defects lead in high low energy luminescence (higher wavelength), besides the contribution of defects states from GaN in superposition with these luminescence yields a higher wavelength yellowish-green DB emission spectra (at 560 nm) [50]. As the thickness of ZnO increases, the concentration of O_V (including Zn_i and O_i) decreases, leading to a strong dominant GL emission at its designated position of ~500 nm [51]. In this scenario, the contribution of O_i (and associated YL emission) is significantly suppressed and the surface reaction doesn't permits migration of atoms due to higher atomic coordination and lower desorption (i.e. increment in overlayer thickness). GL originates from the radiative recombination from the shallow donor levels to deeply trapped holes at O_V and thereby its intensity should be decreased with reduction in O_V (as witnessed via XPS and PL results). Since the shallow donor centres pursue multiple sub-states, a wide spectrum of defect related GL emission (490–550) is obtained [52,53]. The aforementioned explanation divulges the reason behind the observed blue shift in DB (question 1) and indicates that the intensity of DB should also be decreased with overlayer thickness, though an ambiguity was witnessed in the case of 5-ZnO. The position of GL is a reflection of defect states at the surface and interface of the ZnO film. Tay et al. [52] has reported that the GL from ZnO can be identified into two characteristic emissions according to their emission energy (high or low). The higher energy emission (lower wavelength, 504 nm) was attributed to the surface modification/reconstruction via O_V while the lower energy emission (higher wavelength, 550 nm) was ascribed to the O_V in the bulk ZnO. Since interfacial mechanisms (dipoles, BB etc.) were prominent in 2-ZnO & 5-ZnO, it displayed low energy emissions while the emission shifted towards higher energy as the surface modifications/reconstructions became dominant in 8-ZnO & B-ZnO with increment in ZnO thickness. In order to answer the question 2, we have probed the surface and interfacial reactions and defect states in the ZnO/GaN heterostructures. The PL results demonstrate that B-GaN as well as the B-ZnO pursue very small amount of DB and hence the 2-ZnO & 5-ZnO displayed lower intensity of DB. In case of 5-ZnO, the defects states were significant due to lower thickness of ZnO as well lower contribution from GaN, so it yielded higher intensity of DB with respect to 2-ZnO & 8-ZnO.

Finally, correlating the increment in responsivity/detectivity of the fabricated UV PDs with ZnO thickness, we observed that 8-ZnO pursue least amount of defects associated with of O_V and Zn interstitials along with an upwards BB, lowest barrier height and VBO at the interfacial region. The high optical response also divulged suppression of defect states with strong near band edge emission, while I-V curves corresponded to decrease in threshold voltage. The aforementioned explanation indicate that absorption of incident photons and the conduction of photogenerated carriers is prominent in 8-ZnO, which facilitate higher flux density per unit area and thereby yield increases the responsivity. Also, the modulation in barrier height (SBH) across the metal-semiconductor (Au-ZnO/GaN) and semiconductor-semiconductor (ZnO-GaN) interfaces would be dominating in 8-ZnO (due to highest overlayer thickness) which encourages easier carrier transport and limited reverse saturation current density [54] ultimately leading to higher efficiency of the photodetector.

4. Conclusion

The present article demonstrates the dependence of ZnO/GaN based Schottky barrier photodetectors on ZnO overlayer thickness. The overlayer thickness induced perturbations in electronic structure and defects states at ZnO/GaN interface were thoroughly analysed and correlated with device performance. Significant reduction in the contribution of oxygen vacancies (and interstitials) and VBO at the ZnO/GaN interface was perceived with increment in ZnO thickness (from 2 nm to 8 nm). This reduction was attributed to interface dipole strength along with dramatic change in localized BB (downwards-flat-band-upwards). The current conduction was significantly improved with ZnO thickness, though an anomaly in Schottky barrier height and ideality factor was perceived in heterostructure having ZnO thickness of 5 nm. The photodetection measurements divulged a peak responsivity &

detectivity of 225 mA/W^{-1} & 48.3 ($\times 10^{12}$) Jones with a high speed photoswitching (upto 20 ms) and repeatable response for over five photodetection cycles. This studies reveals the underlying interfacial science at the ZnO/GaN interface which would assist in optimizing the performance of ZnO/GaN heterostructure based devices.

Acknowledgement

The authors acknowledge the Director, CSIR-NPL India, for his support. The work is financially supported by the Department of Science and Technology (Govt. of India) under grant aid DST/TM/CERI/C245(G). Monu Mishra would like to thanks CSIR (Govt. of India) for financial support under Senior Research Fellowship scheme. SD acknowledges, Indian Academies (IAS, INSA & NASI) for financial support under SRFP- Teacher fellowship program.

Appendix A. Supplementary data

Supplementary data to this article can be found online at https://doi.org/10.1016/j.apsusc.2019.01.192.

References

[1] B. Zhao, F. Wang, H. Chen, L. Zheng, L. Su, D. Zhao, X. Fang, An ultrahigh responsivity (9.7 mA/W^{-1}) self-powered solar blind photodetectors based on individual ZnO-Ga_2O_3 heterostructures, Adv. Funct. Mater. 27 (2017) 1700264.
[2] Y. Zhang, A. Dadgar, T. Plaacios, Gallium nitride vertical power devices on foreign substrates: a review and outlook, J. Phys. D. Appl. Phys. 51 (2018) 273001.
[3] S.K. Hong, H.J. Ko, Y. Chen, T. Hanada, T. Yao, ZnO/GaN heterointerfaces and ZnO films grown by plasma-assisted molecular beam epitaxy on (0001) GaN/Al_2O_3, J. Vac. Sci. Technol. B 18 (2000) 2313.
[4] C. Chen, M. Dutta, M.A. Stroscio, Confined and interface phonon modes in GaN/ZnO heterostructures, J. Appl. Phys. 95 (2004) 2540.
[5] S.A. Chevtchenko, J.C. Moore, U. Ozgur, X. Gu, A.A. Baski, H. Morkoc, B. Nemeth, J.E. Nause, Comparative study of the (0001) and (000-1) surfaces of ZnO, Appl. Phys. Lett. 89 (2006) 182111.
[6] Y. Zhang, Z.F. Wu, P.F. Gao, D.Q. Fang, S.L. Zhang, Enhanced visible light absorption in ZnO/GaN heterostructured nanofilms, J. Alloys Compd. 704 (2017) 478.
[7] D.K. Hwang, S.H. Kang, J.H. Lim, E.J. Yang, J.Y. Oh, J.H. Yang, S.J. Park, p-ZnO/n-GaN heterostructure ZnO light emitting diodes, Appl. Phys. Lett. 86 (2005) 222101.
[8] F. Schuster, B. Laumer, R.R. Zamani, C. Magen, J.R. Morante, J. Arbiol, M. Strutzmann, p-GaN/n-ZnO heterojunction nanowires: optoelectronic properties and the role of interface polarity, ACS Nano 8 (2014) 4376.
[9] R. Li, P.I. Reyes, S. Ragavendiran, H. Shen, Y. Lu, Tunable surface acoustic wave device based on acoustoelectric interaction in ZnO/GaN heterostructures, Appl. Phys. Lett. 107 (2015) 073504.
[10] M. Miyoshi, S. Fujita, T. Egawa, Demonstration of NOx gas sensing for Pd/ZnO/GaN heterojunction diodes, J. Vac. Sci. Technol. B 33 (013101) (2015).
[11] L. Zhang, F. Zhao, C. Wang, F. Wang, R. Huang, Q. Li, Optoelectronic characteristics of UV photodetector based on GaN/ZnO nanorods *p-i-n* heterostructures, Electron. Mater. Lett. 11 (2015) 682.
[12] C. Chen, J. Yan, C. Lee, High responsivity ultraviolet photodetector based on p-GaN/i-ZnO nanorod/n-ZnO: In Nanorod, ECS Trans. 28 (2010) 27.
[13] H. So, J. Lim, A.J. Suria, D.G. Senesky, Highly antireflective AlGaN/GaN ultraviolet photodetectors using ZnO nanorod arrays on inverted pyramidal surfaces, Appl. Surf. Sci. 409 (2017) 91.
[14] J. Kang, H. Kim, C. Han, H. Yang, S.R. Jeon, B. Park, H. Cha, Enhanced UV absorption of GaN photodiodes with a ZnO quantum dot coating layer, Opt. Express 26 (2018) 8296.
[15] S. Hong, T. Hanada, H. Makino, Y. Chen, H. Ko, A. Tanaka, H. Sasaki, S. Sato, Band alignment at a ZnO/GaN (0001) heterointerfaces, Appl. Phys. Lett. 78 (2001) 3349.
[16] W. Yang, K. Hu, F. Teng, J. Weng, Y. Zhang, X. Fang, High-performance silicon-compatible large-area UV-to-visible broadband photodetector based on integrated lattice-matched type II Se/n-Si heterojunctions, Nano Lett. 18 (2018) 4697.
[17] W. Ouyang, F. Teng, X. Fang, High performance BiOCl nanosheets/TiO_2 nanotube array heterojunction photodetector: the influences of self-induced inner electric fields in the BiOCl nanosheets, Adv. Funct. Mater. 28 (2018) 1707178.
[18] Y. Ning, Z. Zhang, F. Teng, X. Fang, Novel transport and self-powered photodectors based on cross ZnO nanofiber array homojunction, Small 17 (2018) 1703754.
[19] F. Teng, K. Hu, W. Ouyang, X. Fang, Photoelectric detectors based on inorganic p-type semiconductor materials, Adv. Mater. 30 (2018) 1706262.
[20] K. Hu, F. Teng, L. Zheng, P. Yu, Z. Zhang, H. Chen, X. Fang, Laser Photonics Rev. 1 (2017) 11.
[21] D.A. Yarekha, A. Vicet, A. Perona, G. Glastre, B. Fraisse, Y. Rouillard, E.M. Skouri, G. Boissier, P. Grech, A. Joullié, C. Alibert, A.N. Barano, High efficiency GaInSbAs/GaSb type-II quantum well continuous wave lasers, Semicond. Sci. Technol. 15 (2000) 390.
[22] K. Lee, P. Chang, T. Chen, S. Chang, H. Shiu, L. Chang, C. Chen, S. Chang, Synchrotron radiation based cross-sectional scanning photoelectron microscopy and spectroscopy of n-ZnO:Al/p-GaN:Mg heterojunction, Appl. Phys. Lett. 102 (2013) 072104.
[23] T. Nakayama, M. Murayama, Electronic structures of hexagonal ZnO/GaN interfaces, J. Cryst. Growth 214 (2000) 299.
[24] J. Lei, D. Zhu, M. Xu, S. Hu, First-principles simulations of two dimensional electron gas near the interface of ZnO/GaN (0001) superlattice, Phys. Lett. A 379 (2015) 2384.
[25] M. Mishra, S. Krishna, N. Aggarwal, S. Vihari, G. Gupta, Electronic structure analysis of GaN films grown on r- and a-plane sapphire, J. Alloys Compd. 645 (2015) 230.
[26] M. Garg, T.R. Naik, C.S. Pathak, S. Nagrajan, V.R. Rao, R. Singh, Significant improvement in the electrical characteristics of Schottky barrier diodes on molecularly modified gallium nitride surfaces, Appl. Phys. Lett. 112 (2018) 163502.
[27] M. Mishra, A. Gundimeda, S. Krishna, N. Aggarwal, L. Goswami, B. Gahtori, B. Bhattacharya, S. Husale, G. Gupta, Surface engineered nanostructured based efficient nonpolar GaN ultraviolet photodetectors, ACS Omega 3 (2018) 2304.
[28] A. Gundimeda, S. Krishna, N. Aggarwal, A. Sharma, N. Dilawar, K.K. Maurya, S. Husale, G. Gupta, Fabrication of nonpolar GaN based highly responsive and fast UV photodetector, Appl. Phys. Lett. 110 (2017) 103507.
[29] T. Li, D. Mario, Non-resonant below-bandgap two-photon absorption in quantum dot solar cells, Appl. Phys. Lett. 106 (2015) 171101.
[30] H. Zhou, P. Gui, Q. Yu, J. Mei, H. Wang, G. Fang, Self-powered, visible-blind ultraviolet photodetector based on n-ZnO nanorods/i-MgO/p-GaN structure light-emitting diodes, J. Mater. Chem. C 3 (2015) 990.
[31] H. Zhou, P. Gui, L. Yang, C. Ye, M. Xue, J. Mei, Z. Song, H. Wang, High performance self-powered ultraviolet photodetector based on a ZnO nanoarray/GaN structure with a CdS insert layer, New J. Chem. 41 (2017) 4901.
[32] D. Liu, H. Li, J. Gao, S. Zhao, Y. Zhu, P. Wang, D. Wang, A. Chen, X. Wang, J. Yang, High performance ultraviolet photodetector based graphene quantum dots decorated ZnO nanorods/GaN film isotype heterojunctions, Nanoscale Res. Lett. 13 (2018) 261.
[33] J.K. Sheu, M.L. Lee, C.J. Tun, S.W. Lin, Ultraviolet band-pass Schottky barrier photodetectors formed by Al-doped ZnO contacts to n-GaN, Appl. Phys. Lett. 88 (2006) 043506.
[34] D. Shao, M. Yu, J. Lian, S.M. L, Ultraviolet photodetectors fabricated from multi-walled carbon nanotubes/Zinc oxide/p-GaN composite structure, IEEE Electron Dev. Lett. 34 (2013) 1169.
[35] M. Mishra, A. Gundimeda, S. Krishna, N. Aggarwal, B. Gahtori, N. Dilawar, V. Agrawal, M. Singh, R. Rakshit, G. Gupta, Wet chemical etching induced stress relaxed nanostructures on polar and non-polar epitaxial GaN films, Phys. Chem. Chem. Phys. 19 (2017) 8787.
[36] M. Mishra, S. Krishna, N. Aggarwal, M. Kaur, S. Singh, G. Gupta, Pit assisted oxygen chemisorption on GaN surfaces, Phys. Chem. Chem. Phys. 17 (2015) 15201.
[37] J. Wang, Z. Wang, B. Huang, Y. Ma, Y. Liu, X. Qin, X. Zhang, Y. Dai, Oxygen vacancy induced band-gap narrowing and enhanced visible light photocatalytic activity of ZnO, ACS Appl. Mater. Interfaces 4 (2012) 4024.
[38] M. Mishra, S. Krishna, N. Aggarwal, G. Gupta, Surface chemistry and electronic structure of nonpolar and polar GaN, Appl. Surf. Sci. 345 (2015) 440.
[39] H.W. Jang, J.H. Lee, J.L. Lee, Characterization of band bending on Ga-face and N-face GaN films grown by metal organic chemical-vapour deposition, Appl. Phys. Lett. 80 (2002) 3955.
[40] D. Segav, C.G. Van de Walle, Origins of Fermi-level pinning on GaN and InN polar and nonpolar surfaces, Europhys. Lett. 76 (2006) 305.
[41] Z. Zhang, J.T. Yates Jr., Band bending in semiconductors: chemical and physical consequences at surfaces and interfaces, Chem. Rev. 112 (2012) 5520.
[42] N. Goyal, B. Iniguez, T.A. Fjeldly, Analytical modelling of bare surface barrier height and charge density in AlGaN/GaN heterostructure, Appl. Phys. Lett. 101 (2012) 103505.
[43] J.W. Liu, A. Kobayashi, S. Toyoda, H. Kamada, A. Kikuchi, J. Ohta, H. Fujioka, H. Kumigashira, M. Oshima, Band offsets of polar and nonpolar GaN/ZnO heterostructures determined by synchrotron radiation photoemission spectroscopy, Phys. Status Solidi B 248 (2011) 956.
[44] P.A. Rodnyi, I.V. Khodyuk, Optical and luminescence properties of zinc oxide, Opt. Spectrosc. 111 (2011) 776.
[45] S. Krishna, N. Aggarwal, M. Mishra, K.K. Maurya, S. Singh, N. Dilawar, S. Nagarajan, G. Gupta, Correlation of growth temperature with stress, defect states and electronic structure in an epitaxial GaN film grown on *c*-sapphire via plasma MBE, Phys. Chem. Chem. Phys. 18 (2016) 8005.
[46] S. Krishna, N. Aggarwal, A. Reddy, P. Dugar, M. Mishra, L. Goswami, N. Dilawar, M. Kumar, K.K. Maurya, G. Gupta, Probing the correlation between structure, carrier dynamics and defect states of epitaxial GaN film on (1120) sapphire grown by rf-molecular beam epitaxy, RSC Adv. 5 (2015) 73261.
[47] S. Jeong, S.K. Oh, J. Ryou, K. Ahn, K.M. Song, H. Kim, Monolithic inorganic ZnO/GaN semiconductors heterojunction white light emitting diodes, ACS Appl. Mater. Interfaces 10 (2018) 3761.
[48] M.A. Reshchikov, H. Morkoc, B. Nemeth, J. Nause, J. Xie, B. Hertog, A. Osinsky, Luminescence properties of defects in ZnO, Phys. B 401 (2007) 358.
[49] C.G. Van de Valle, J. Neugebauer, First principle calculations for defects and impurities: applications to III-nitrides, J. Appl. Phys. 95 (2004) 3851.
[50] F.H. Bo, Y.S. Yan, Z.P. Feng, W.H. Yuan, L.X. Lin, J.C. Mei, Z.Q. Sheng, C.Y. Hai, W.Z. Guo, Investigation of oxygen vacancy and interstitial oxygen defects in ZnO films by photoluminescence and x-ray photoelectron spectroscopy, Chin. Phys. Lett. 24 (2007) 2108.
[51] D. Liu, Y. Lv, M. Zhang, Y. Liu, Y. Zhu, R. Zong, Y. Zhu, Defect related luminescence and photocatalytic properties of porous ZnO nanosheets, J. Mater. Chem. A 2 (2014) 15377.

[52] Y.Y. Tay, T.T. Tan, M.H. Liang, F. Boey, S. Li, Specific defects, surface band bending and characteristic green emissions of ZnO, Phys. Chem. Chem. Phys. 12 (2010) 6008.
[53] M. Garg, T.R. Naik, C.S. Pathak, S. Nagrajan, V.R. Rao, R. Singh, Significant improvement in the electrical characteristics of Schottky barrier diodes on molecularly modified gallium nitride surfaces, Appl. Phys. Lett. 112 (2018) 163502.
[54] Q. Chen, J.W. Yang, A. Osinsky, S. Gangopadhyay, B. Lim, M.Z. Anwar, M.A. Khan, D. Kuksenkov, H. Temkin, Low noise p-π-n GaN ultraviolet photodetectors, Appl. Phys. Lett. 70 (1997) 2277.